RESEARCH ARTICLE

physica status solidi pss a
www.pss-a.com

Tip Modification for Interaction Studies Between Polysaccharides and Dental Materials

*Swen Ehnert, Christine Müller-Renno, Matthias Hannig, and Christiane Ziegler**

Neutral polysaccharides, such as bacterial dextrans, are one of the main components of the oral conditioning film, which is the first step in the formation of microbial biofilms on dental materials in the oral cavity. Although they play an essential role alongside proteins, their adhesion mechanisms are still very unknown. Therefore, they are currently being studied using various analytical methods. In particular, by means of scanning force spectroscopy (SFS), the adhesion forces are to be measured as a function of multiple parameters such as pH value or surface material. Cantilever tips must therefore be modified with the polysaccharide of interest. A stable coupling of dextran, which serves as a model polysaccharide here, can be achieved by a photochemical modification method, which is verified by fluorescence microscopy, X-ray photoelectron spectroscopy, scanning force microscopy, and SFS.

1. Introduction

Inflammation in the oral cavity and dental disease results from microbial biofilms (plaque) colonizing teeth or dental implant and restorative materials.[1–7] Biofilm formation occurs through the adsorption of microorganisms to a previously formed bacteria-free conditioning film (pellicle), consisting of (unspecifically) adsorbed biopolymers.[6–10] In addition to proteins, polysaccharides, such as dextrans, a family of bacterial, neutral, and variously branched α–glucans (**Figure 1**), have also been identified in the pellicle.[10–13] The adsorption of biopolymers is a complex interplay driven by van der Waals interactions, Coulomb interactions, hydrogen bonding, hydrophobic interactions, conformational changes, de/solvation processes, and lateral interactions between neighboring polymers.[14–17] The interaction is strongly influenced by external parameters such as temperature, pH, ionic strength, or buffer composition, as well as surface parameters such as surface energy, polarity, charge, and morphology.[14] In addition, the specific attachment of bacteria to certain molecules, such as bacterial exopolysaccharides incorporated into the pellicle, is possible. Therefore, pellicle composition likely influences plaque formation. Control over the processes involved in pellicle formation could thus also mean control over plaque formation, which is of great clinical importance to avoid dental and implant diseases. Therefore, a comprehensive understanding of biopolymer–substrate and biopolymer–biopolymer interactions must be achieved.

The protein–substrate and protein–protein interactions on dental materials have already been very well investigated. For this purpose, proteins found in saliva, such as bovine serum albumin (BSA) and lysozyme, were used and examined by a multi-method approach of dynamic contact-angle analysis,[18,19] quartz crystal microbalance analysis (QCM),[18] time-of-flight secondary-ion mass spectrometry,[20,21] and biochemical methods (bicinchoninic acid (BCA) assay[22], enzyme activity[23])[19,24–26] to characterize adsorbed biopolymer layers on different dental materials. Also, extensive investigations were carried out using scanning force spectroscopy (SFS) to determine adhesion forces as a function of the pH value, the substrate, or a preadsorbed biopolymer layer.[19,27–29]

In contrast to proteins, the study of the interaction of polysaccharides with dental materials is still significantly underrepresented. We are therefore conducting corresponding investigations using dextran, which is present in the oral biofilm, as a model polysaccharide. In addition to QCM, scanning force microscopy (SFM), fluorescence microscopy, and biochemical quantification assays (phenol-sulfuric acid (PSA) assay[30–32], sulfuric acid-ultraviolet absorption (SA-UV) assay[33]), also the adhesion forces are to be measured using SFS as a function of various parameters such as pH value or substrate. The principle of adhesion force measurement is to "force" a biopolymer to interact with a surface by "pushing" it onto the substrate surface via a biopolymer-modified cantilever tip. The force of this interaction is then measured in terms of cantilever deflection by subsequently "pulling" the molecules from the surface. For this, it is necessary to bind dextran molecules reproducibly to the tip of an SFM cantilever. To immobilize molecules, selected functional groups are covalently or ionically attached to activated surfaces via selective linker molecules (crosslinker).[34–36] However, neutral polysaccharides such as dextran contain almost

S. Ehnert, C. Müller-Renno, C. Ziegler
Department of Physics and Research Center OPTIMAS
University of Kaiserslautern
Erwin Schrödinger Straße 56, 67663 Kaiserslautern, Germany
E-mail: cz@physik.uni-kl.de

M. Hannig
Clinic of Operative Dentistry, Periodontology and Preventive Dentistry
Saarland University Hospital
66421 Homburg, Germany

The ORCID identification number(s) for the author(s) of this article can be found under https://doi.org/10.1002/pssa.202200834.

DOI: 10.1002/pssa.202200834

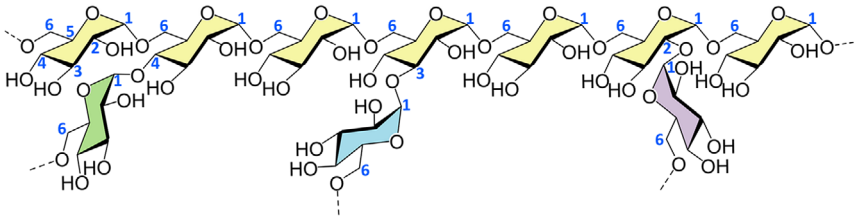

Figure 1. The general structure of dextrans consisting of a continuous $\alpha-1,6$ glycosidically linked backbone (yellow) as well as $\alpha-1,2$ (purple), $\alpha-1,3$ (blue), and $\alpha-1,4$ (green) linked branches.[13]

exclusively hydroxyl groups (OH) with low reactivity. Only at the reducing end and only in the thermodynamically unfavored, open-chain form of the terminal glucose unit, there is a single reactive aldehyde group (CH=O).[37] For example, for a 70 kDa dextran with about 432 glucose units, the ratio OH: CH=O is 1296:1. The aldehyde group is, thus, generally difficult to access for solid surface coupling and needs liquid-phase derivatization beforehand.[38]

The attachment of polysaccharides for, for example, the investigation of force-induced conformational changes in polysaccharides,[39–42] the production of bio-sensitive surfaces for stable lipid–protein bilayer deposition,[43] an electrochemical assay for the investigation of cell-bound carbohydrates,[44] or carbohydrate arrays (glycoarrays) as a tool for studying carbohydrate-binding proteins and carbohydrate-processing enzymes are already described in the literature.[45,46] However, immobilization only took place on bulk surfaces and primarily via either small, short-chain oligosaccharides with better accessible aldehyde groups or previously derivatized polysaccharides, for example, for biotin–streptavidin coupling.[39] For interaction studies with solid surfaces, derivatization is not an option as it would alter the interaction properties of the polysaccharide. In some cases,[40,41] polysaccharides were bound non-covalently to glass surfaces (silicon oxide surface) simply by incubation in the appropriate polysaccharide solution. As there are no other functional groups than the OH groups, this type of immobilization can only act via physisorption by hydrogen bonds. It is known that hydrogen bonding as well as polysaccharide adsorption to mineral surfaces (metal oxide or metal-hydroxylated surfaces) is strongly dependent on pH.[47–49] Thus, it is uncertain how pH-stable this immobilization is and whether it would withstand a series of measurements at different pH values, or whether the pH value affects the amount of immobilized polysaccharide molecules on the tip during the experiment and thus eliminating the comparability of results between different pH values. A single reference was found describing the covalent modification of cantilevers.[50] However, they also only used oligosaccharides that were derivatized at the reducing end and tipless cantilevers, with which no SFS measurements were done.

One way to ensure quick and easy dextran binding without prior derivatization is to use a photolabile linker (photo-linker), as presented by Elender, Kühner, and Sackmann to attach 500 kDa dextran to amino-functionalized surfaces via the amino-selective nitrophenyl azide ANB-NOS (*N*-5-Azido-2-nitrobenzoyloxysuccinimide).[43]

We here present our method for the photochemical attachment of simple and non-derivatized neutral polysaccharides (here, 70 kDa dextran, DEX70) to amino-functionalized surfaces using the more modern amino-selective and photoreactive linker succinimidyl-diazirine (SDA, NHS-diazirine (NHS = *N*-hydroxysuccinimide ester), or succinimidyl 4,4′-azipentanoate), which shows better photostability and more efficient activation.[51–53] The covalent bonds formed by this method are amide bonds (peptide bonds) between the SDA succinimidyl groups and the amino groups of the surface as well as single C–C or C–O bonds between the SDA diazirine groups and the dextran molecules. These bonds are highly stable over a wide range of pH and can only be broken under extreme conditions.[54–56] The modification steps were verified on bulk silicon wafer pieces by SFM, fluorescence microscopy, and X-ray photoelectron spectroscopy (XPS). First SFS experiments with DEX70-modified cantilever tips are presented. The obtained force distance curves as well indicate the successful tip modification. The results now allow to study the interaction between neutral polysaccharides and typical dental materials such as dental gold, dental titanium, and dental ceramics by SFS adhesion force measurements.

2. Results and Discussion

2.1. Surface and Tip Modification

Most cantilevers for SFM/SFS are made of silicon (Si) or silicon nitride (Si_3N_4), both with a native oxide layer (SiO_x).[36] The silicon surfaces are activated for modification by silanization chemistry, for example, with aminoalkyl-substituted silyl ethers such as 3-aminopropyltriethoxysilane (APTES).[35,36,57–59] These molecules bind covalently to the silanol groups (Si–OH) of the native oxide layer in a condensation reaction. The strategy for our photochemical modification with dextran is shown in **Figure 2** (and detailed more in Figure S1, Supporting Information). To optimize the process, flat silicon wafers were used because they allow microscopic control. The first step is to prepare an amino-functionalized silicon substrate and activate it with APTES. Prior to the modification, the silicon surfaces were first cleaned using a three-step, ultrasonically assisted solvent treatment and then activated with oxygen plasma to generate a high concentration of silanol groups to facilitate the APTES coupling reaction.[35,59] The controlled and uniform deposition of the APTES molecules can then be achieved from the gas phase.[58–60] Subsequently, the amino-selective photo-linker SDA is coupled, which finally reacts with DEX70 under UV light irradiation. After each step, samples were analyzed by SFM, fluorescence microscopy, and, in some cases, XPS to demonstrate successful derivatization. For fluorescence microscopy, Si–NH_2 samples were

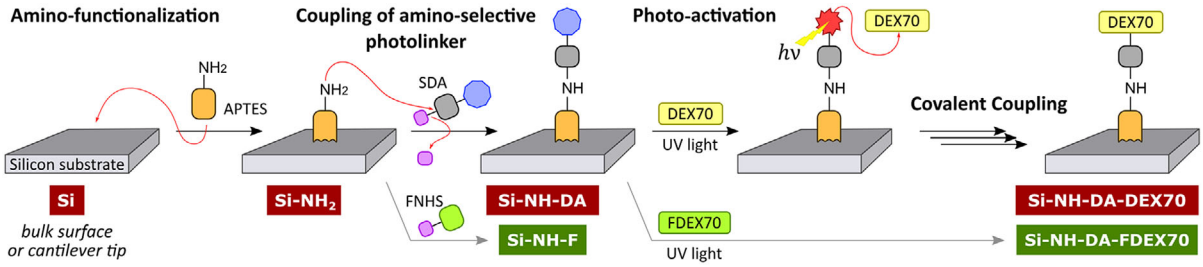

Figure 2. Schematic representation of the photochemical modification method with dextran (including the routes for the attachment of fluorescent compounds).

reacted either with NHS-fluorescein (FNHS) or first with SDA and afterward with fluorescein-isothiocyanate (FITC)-conjugated DEX70 (FDEX70).

For SFS measurements, the silanization step was later avoided, and commercial cantilevers with amino-prefunctionalized colloidal probes were directly modified with SDA and DEX70.

2.2. SFM

The verification by SFM was carried out by comparing surface topography parameters and layer thicknesses (determined by the scratch method, see Section S2, Supporting Information) after each modification step. **Table 1** represents the results of

Table 1. Results of the SFM investigations: representation of height images, surface topography parameters, line profiles, and layer thicknesses.

Parameter[a]	Si clean	Si–NH_2	Si–NH–DA	Si–NH–DA–DEX70
	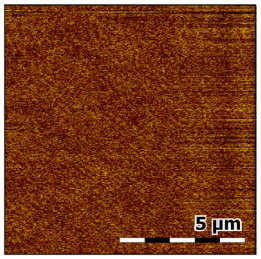	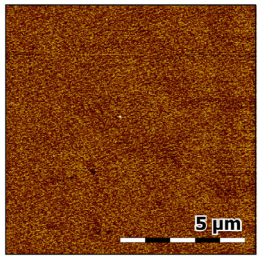	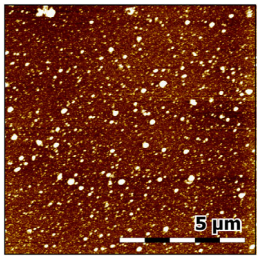	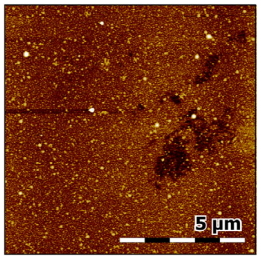
Sq [nm][b]	0.11 ± 0.001	0.19 ± 0.005	1.89 ± 0.148	0.84 ± 0.282
Sp [nm][c]	1.4 ± 0.1	5.3 ± 3.8	57.9 ± 21.4	48.2 ± 40.9
Sz [nm][d]	2.2 ± 0.4	6.1 ± 3.8	60.3 ± 20.6	50.6 ± 41.0
Sdr [%][e]	0.005 ± 0.0001	0.013 ± 0.0004	0.136 ± 0.0090	0.077 ± 0.0114
	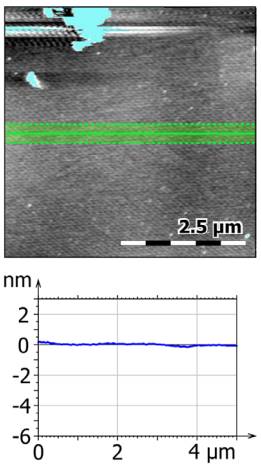	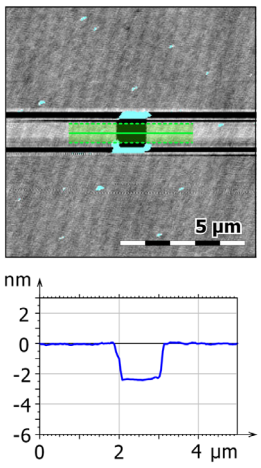	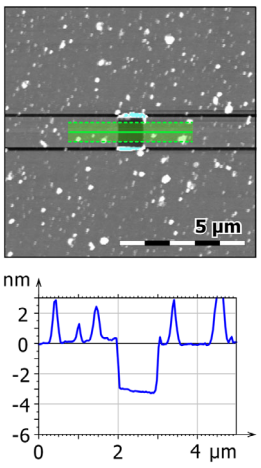	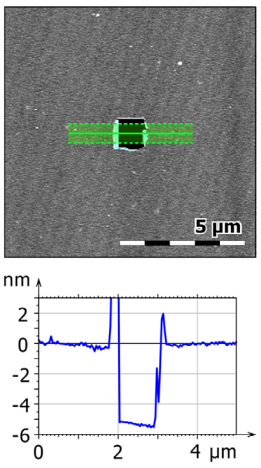
Layer thickness [nm]	–	2.4 ± 0.2	3.5 ± 0.3	5.3 ± 0.1

[a]Scan sizes are 10 × 10 μm² (5 μm scale bars), except for the scratched image of Si clean, which is 5 × 5 μm² (2.5 μm scale bar); light blue areas are not-measured points due to the threshold adjustment. [b]*Sq* = root mean square height. [c]*Sp* = maximum peak height. [d]*Sz* = maximum height (peak-to-valley); and. [e]*Sdr* = developed area (hybrid parameter).

the SFM investigation. The SFM images of Si–NH_2 show only marginally increased *Sq* and *Sdr* values (for definition see Table 1, footnotes) compared to the clean silicon substrate, indicating a very smooth APTES layer without agglomerates after 30 min of gas-phase silanization. The layer thickness is about 2.4 nm, which is around five times the length of a single APTES molecule (0.5 nm),[60] showing that it is not yet a monolayer. Since the layer smoothness and thickness were very well reproducible, the incubation time of 30 min was kept (and not optimized for smaller layer thickness) for the subsequent reaction steps. Here, the layer thicknesses increase with each step and thus indicate the successful binding of molecules. Upon SDA coupling, the *Sq* and *Sdr* values increase sharply, likely due to the agglomeration of SDA molecules. This can also be seen from the significantly higher *Sp* and *Sz* values (for definition, see Table 1, footnotes). The subsequent reaction with DEX70, in turn, leads back to a lower roughness. However, the increase in layer thickness does not correlate with the (hydrodynamic) diameter of a random-coil dextran molecule of about 13 nm.[61] Thus, dextran appears to spread out flat and to, at least partially, level out the unevenness of the previous surface. Nevertheless, some agglomerates are still present, which can be seen from the still relatively high *Sp* and *Sz* values.

2.3. Fluorescence Microscopy

The reaction of Si–NH_2 with FNHS (Si–NH–F) and Si–NH–DA with FDEX70 (Si–NH–DA–FDEX70) provided the point-like fluorescence in **Figure 3**. FNHS was chosen because it has the same amino-selective NHS ester group as the photo-linker SDA. Thus, the fluorescent dots are indeed caused by the agglomeration of FNHS on the Si–NH_2 surface, as could already be detected for SDA by SFM (previous subsection). On the Si–NH–DA sample, the SDA agglomerates probably lead to a greater extent of FDEX70 binding. However, continuous homogenous coverage between the agglomerates was observed by SFM. This indicates that there is also fluorescent material between the luminous dots, but its fluorescence is too weak to be detected. The fluorescence images are therefore considered proof of successful modification.

2.4. XPS

A cleaned silicon (Si) sample as well as the functionalized samples Si–NH_2 and Si–NH–DA were analyzed by XPS (**Figure 4**). The clean Si surface has no nitrogen and only low concentrations of carbon, which can be attributed to the typical adventitious carbon always found on surfaces prepared under ambient conditions.[62] Silicon and oxygen, which come from the bulk material and the native oxide layer, make up the majority. After the reaction with APTES (Si–NH_2), a clear nitrogen signal is detected. In addition, the carbon content significantly increases while the silicon content decreases. This indicates that the Si surface is covered by an organic and nitrogen- and carbon-containing APTES layer. With SDA coupling (Si–NH–DA), there is only a negligible increase in the nitrogen concentration, but again there is a significant increase in the carbon concentration and a decrease in the silicon concentration, pointing to an additional layer formation with organic material.

The C 1s and N 1s chemical states are crucial for checking the chemical modification steps. A detailed table of all determined states as well as the O 1s and Si 2p detail spectra can be found in Supporting Information (Section S3, Supporting Information). The clean Si sample shows the typical C 1s signal

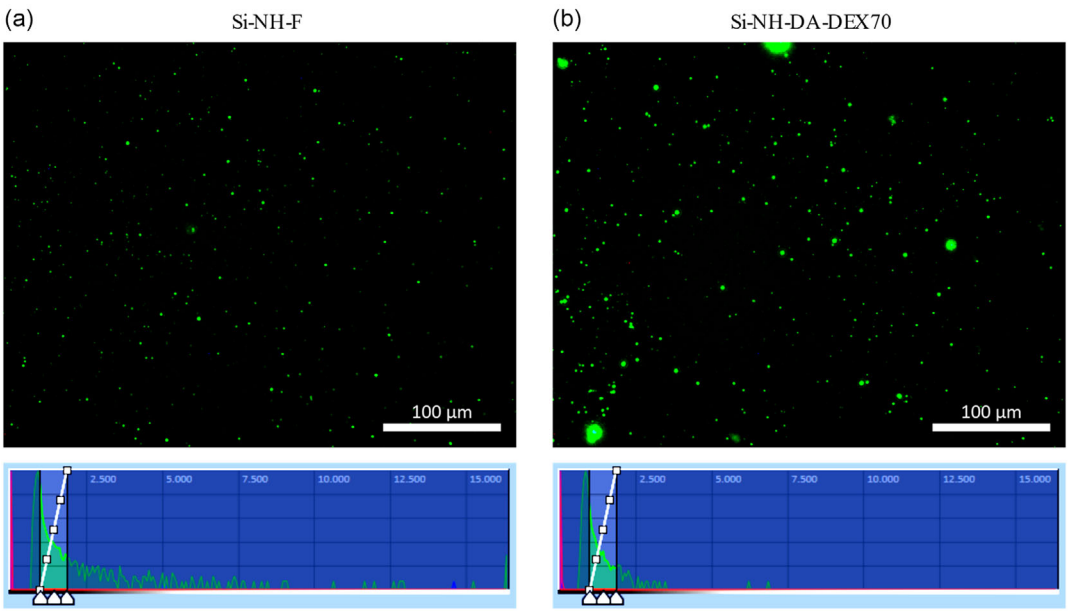

Figure 3. Fluorescence images and intensity histograms showing a) successful gas-phase amino-silanization as well as successful coupling between the amine and the amino-selective NHS-ester required for photo-linker attachment, and b) successful photochemical attachment of FITC-conjugated 70 kDa dextran (FDEX70) to an SDA-modified silicon surface (5 s exposure time, 100 µm scale bar).

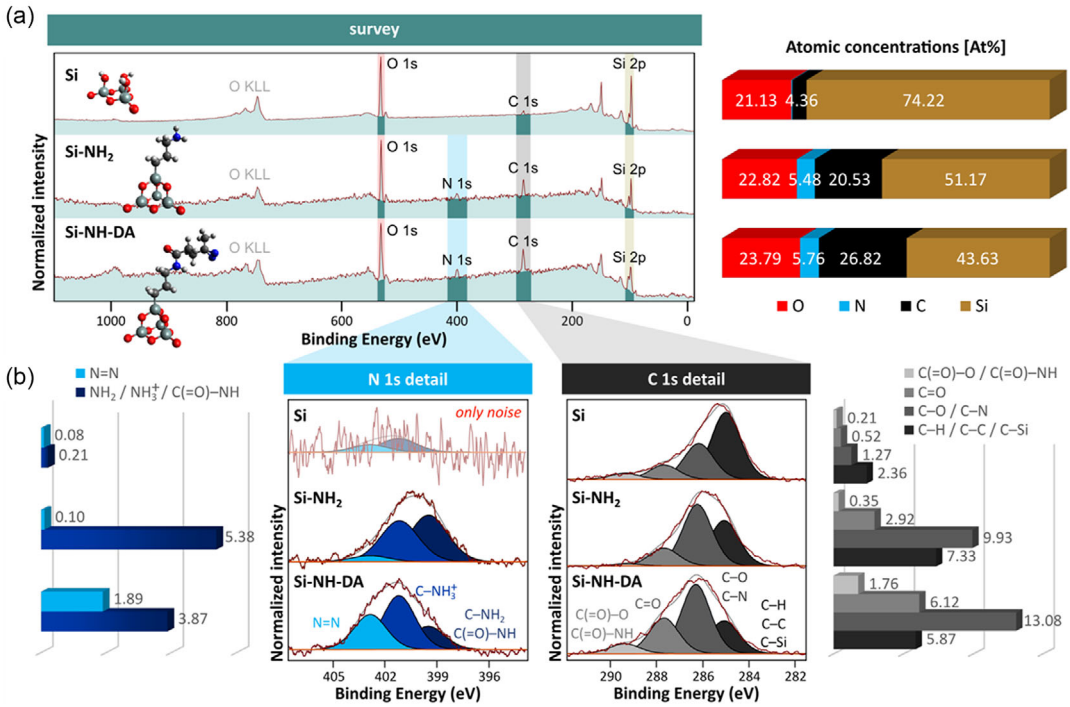

Figure 4. Results of the X-ray photoelectron spectroscopy (XPS) analysis: a) survey spectra and surface element compositions, and b) C 1s and N 1s detail spectra and chemical bonding states (ball-and-stick molecular structures visualized with Avogadro software:[75,76] = silicon, = carbon, = nitrogen, = oxygen, and = hydrogen).

of the adventitious carbon already mentioned earlier.[62] After gas-phase silanization (Si–NH_2), the C 1s spectrum shows a significant increase in the C–C (285.0 eV) and C–N (286.2 eV) bonding states compared to the clean Si sample, reflecting the organic aminopropyl moiety [–$(CH_2)_3$–NH_2] of the deposited APTES molecules.[63] The N 1s spectrum shows peaks for organic amine –NH_2 (399.5 eV)[63,64] and ammonium –NH_3^+ (401.2 eV).[64–66] The latter probably forms after the preparation by reaction of the free, strongly basic amines with water from the air or when rinsing the samples.[67] Amine and ammonium together account for about 98% of the total nitrogen signal. As expected, no other bonding states can be found since only the amino groups of the APTES molecules contribute to the nitrogen signal. The binding of SDA (Si–NH–DA) provides an N 1s spectrum in which the proportion of amine and ammonium together has decreased significantly to about 67%. With a contribution of about 33%, a new signal at 402.9 eV is now clearly visible. During the reaction, the amine/ammonium groups of the APTES molecules should be converted to amides [–C(=O)NH–] by reaction with the NHS ester groups of the SDA, and the diazirine group (a three-membered heterocycle with –N=N–) should be introduced. Since the N 1s signal of the amide also has an energy of about 400 eV, similar to the free amine,[63] the new signal has to originate from the diazirine. Examples of organic nitrogen compounds that are detected around 402–403 eV are cyanide (–C≡N) or azomethane (H_3C–N=N–CH_3),[63] that is, molecules with C,N- or N,N-multiple bonds such as the diazirine N,N-double bond detected here. A further significant change in the N 1s detail spectrum can be observed during the SDA coupling, which can be interpreted as an indication of a successful photo-linker connection. In the C 1s spectrum, the proportion of the C–N bonding state (286.2 eV) also increases, which is probably due to the carbon of the three-membered diazirine ring. There is also an increase in the signal at 289.3 eV, which is most probably related to the carbonyl carbon from the amide [–C(=O)–NH–],[63] already mentioned earlier.

2.5. SFS

SFS measurements were performed with both the amino-prefunctionalized PT.GS.AU.NH3 (manufacturer term, see Experimental Section for details) and the DEX70-modified PT.GS.AU.NH–DA–DEX70 cantilevers. The results of the prefunctionalized cantilever are necessary as they serve as a reference for the DEX70 coupling control. Solvent-cleaned silicon wafers with very low roughness (Sq = 0.11 nm) were used as the model substrates to avoid topographical effects. The SFS measurements were carried out in sodium phosphate–buffered saline (pH 7, ionic strength 100 mM) with a trigger force of 1 nN and a dwell time of 10 s. Exemplary force–distance curves (in short: force curves) from different positions of the same substrate showing apparent differences between the two functionalizations are represented in **Figure 5**a. PT.GS.AU.NH3 delivered peaks at low forces and short rupture lengths, which are probably due to interaction with the thin amino-functionalized layer or the cantilever tip itself (tip adhesion). The mean tip-corrected adhesion force is 0.37 ($\pm$0.28) $\times 10^{-4}$ N m^{-1} (94 $\pm$ 70 pN without tip-correction) at an averaged rupture length of 4.7 ($\pm$3.2) nm. PT.GS.AU.NH–DA–DEX70, in

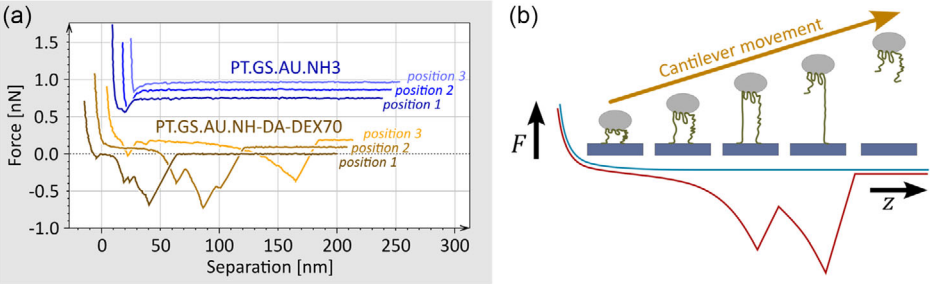

Figure 5. Results of the scanning force spectroscopy (SFS) measurements on silicon: a) exemplary force-distance curves for PT.GS.AU.NH3 and PT.GS.AU.NH–DA–DEX70 from three different positions (illustrated by the different color shades) of the same substrate, respectively, and b) postulated interaction mechanism of different length DEX70 segments resulting in sawtooth-shaped force curves.

contrast, delivered pronounced isolated or sawtooth-like peaks at significantly higher forces and rupture lengths. With a value of 1.86 $(\pm 0.91) \times 10^{-4}$ N m^{-1} (466 ± 229 pN without tip correction), the mean adhesion force is about half an order of magnitude higher. The corresponding averaged rupture length is 36.8 (±30.9) nm and thus about one order of magnitude larger.

Watching the rupture lengths of PT.GS.AU.NH–DA–DEX70, they occur randomly but always below about 200 nm, which is basically what would be expected from a single DEX70 molecule. With a glucose monomer length of 495 pm[68,69] and 394 monomers for the dextran backbone ($M_r = 70$ kDa), the total length of the molecule is about 195 nm (see Supporting Information, Section S4, Supporting Information). Considering the whole molecular weight range specified by the manufacturer ($M_r \approx 60$–80 kDa), the maximum rupture lengths can be 167–223 nm, but only if the DEX70 molecule is terminally attached to the tip. However, due to the photochemical attachment, the probability is significantly higher, that the molecule is bound to the tip unselectively, that is, with random positions of the molecular chain, which results in many shorter segments of different lengths available for interaction. This would not only explain the scattering of the rupture lengths but also the sawtooth-like shape of many force curves. In general, sawtooth-shaped force curves are primarily known from proteins.[70,71] They are caused by unfolding mechanisms or ligand-receptor systems in which relatively strong intra- or intermolecular interactions are broken by the retraction force. In the case of neutral polysaccharides, such as dextran, only weak hydrogen bonds between the OH groups (O–H···O–H) exist. A sawtooth shape would, therefore, not necessarily be expected. However, this may be caused by a sudden opening of coils or loops. But it is more likely that several of these different length segments mentioned earlier interact with the substrate and rupture at different times (Figure 5b).

3. Conclusion

A method for the photochemical, covalent attachment of dextran to amino-prefunctionalized surfaces was presented. This was proven by several analytical tools. SFM showed that the surface topography changes and the layer thickness increases with each step. The successful coupling could also be confirmed by fluorescent markers. Furthermore, the chemical coupling steps could be verified by XPS based on the analysis of the carbon and nitrogen concentrations and of the N 1s chemical states.

The successful modification of the colloidal cantilever tip could be clearly verified by SFS measurements. Clear adhesion peaks can be observed in the force-distance curves with reasonable rupture lengths, which are caused by the interaction of DEX70 segments with the silicon surface. The comparison with the prefunctionalized cantilevers shows a significant increase in the adhesion force and the rupture length after modification with DEX70.

Our method is not limited to dextran or cantilever modification but can also be used in general to immobilize neutral, uncharged polysaccharides on amino-prefunctionalized surfaces without using specific linkers such as biotin and streptavidin. In this respect, the method can also be very interesting for other applications in areas such as biosensors, soft materials, or medicine.

4. Experimental Section

Reagents and Materials: Aceton p.A. (≥99.8%) and isopropanol p.A. (2-propanol, ≥ 99.7%) were purchased from VWR (Wayne, PA, USA). Ultrapure water (18.2 MΩ cm^{-1}) was prepared by the MerckMillipore Milli-Q Reference A + System (Merck KGaA, Darmstadt, Deutschland). Dimethylformamide (DMF, 99.8%, ExtraDry, stored over molecular sieve, AcroSeal, Acros Organics), APTES (99%, dry, stored under nitrogen, AcroSeal, Acros Organics), NHS-diazirine (SDA, succinimidyl 4,4′-azipentanoate, ≥90%, 3.9 Å Spacer, UV activation 330–370 nm, Pierce Biotechnology), and FNHS (5/6-carboxyfluorescein succinimidyl ester, 5/6-FAM SE, >90.0%, Pierce Biotechnology) were purchased from Thermo Fisher Scientific GmbH (Waltham, MA, USA). DEX70 (M_r 60 000–80 000 Da, from *Leuconostoc spp.*), FITC-conjugated dextran 70 kDa (FITC-Dextran, FDEX70, M_r 60 000–76 000 Da, from *Leuconostoc mesenteroides*), sodium chloride (NaCl, ≥99.5%, BioXtra), sodium dihydrogen phosphate monohydrate ($NaH_2PO_4 \cdot H_2O$, ≥99.0%), and disodium hydrogen phosphate (Na_2HPO_4, ≥ 99.0%) were purchased from Sigma-Aldrich/Merck KGaA (Darmstadt, Germany). All the materials that met the surfaces or the cantilevers were cleaned in a laboratory dishwasher at 80 °C with a subsequent automatic rinse with distilled water and additionally with residual air plasma (50 W) for 5 min directly before use. Plasma cleaning and activation were performed in the Pico low-pressure plasma system from diener electronic GmbH & Co. KG (Ebhausen, Germany).

Silicon Surfaces: Silicon wafers with a native oxide layer (Czochralski method, crystal orientation (100), orientation accuracy ± 0.5°, thickness 500–550 µm, one-side polished, type p, boron-doped, resistance

1–5 Ωcm) were purchased from Si-Mat Silicon Materials (Kaufering, Germany). Small wafer pieces were prepared by coating with a protective photoresist and cutting with a wafer saw at the Nano Structuring Center (NSC) of the University of Kaiserslautern (Germany). Directly before use, the photoresist was removed by intensive rinsing with acetone, and the surfaces were cleaned by ultrasound-assisted solvent treatment in acetone, isopropanol, and ultrapure water for 10 min each. After each step, the samples were thoroughly rinsed with the respective solvent. The surfaces were dried in a stream of inert gas (nitrogen or argon) and activated with oxygen plasma (50 W, 10% O_2) for 2 min. Silicon surfaces for SFM imaging were left after plasma treatment for several days, thoroughly rinsed with ultrapure water, and blown off with dry, oil-free compressed air. Silicon surfaces as substrates for SFS measurements were not plasma-cleaned.

Surface Modification: Gas-phase amino-functionalized silicon surfaces (Si–NH_2) were prepared by incubating the silicon substrates for 30 min under an inert argon atmosphere and a reduced pressure of 200 mbar near an 80 °C heated petri dish (∅ = 40 mm) filled with 0.5 mL APTES. Si–NH_2 samples were cured on a hot plate (100–120 °C) for 30 min, rinsed thoroughly with isopropanol and ultrapure water, and dried on the hotplate (100–120 °C) for 30 s. For the preparation of Si–NH–DA and Si–NH–F, the Si–NH_2 samples were covered with 900 µL sodium phosphate buffer (100 mM, pH 8.3), 100 µL of a 1–2 mg mL^{-1} solution of the photo-linker SDA or the fluorescence marker FNHS in dry DMF was added, and the solution was gently mixed by pipetting up and down. The samples were incubated in the dark for 1 h at 200 rpm (Microplate Shaker PMS-1000i, Grant Instruments Ltd, Shepreth, Cambridgeshire, UK), then rinsed thoroughly with isopropanol and ultrapure water, and dried on a hot plate (80 °C) for 30 s. For the preparation of Si–NH–DA–DEX70 and Si–NH–DA–FDEX70, the Si–NH–DA samples were covered inside a petri dish (∅ = 40 mm) with 1–2 mL of an aqueous 20 g L^{-1} DEX70 or FDEX70 solution and irradiated with blue UV–A light (365 nm) for 30 min. The irradiation was carried out using a mercury vapor lamp (HBO 103 W/2 10×1, OSRAM, München, Deutschland) integrated into the ZEISS microscope Axioskop 2 MOT (Carl Zeiss Microscopy, Oberkochen, Deutschland) through the ZEISS filter set 01 (item no. 488001-9901-000, excitation BP 365/12, beam splitter FT 395, emission LP 397) and the ZEISS objective Plan-Neofluar 20×/0.50 Ph 2 (item no. 420 351-9910-000). Finally, the samples were rinsed thoroughly with isopropanol and ultrapure water, and dried on a hot plate (80 °C) for 30 s. All samples were either processed directly, characterized, or stored under an argon atmosphere until further use. Si–NH–DA and Si–NH–F samples were additionally stored in the dark.

Tip Modification: The colloidal, amino-prefunctionalized cantilevers "PT.GS.AU.NH3" (manufacturer term for cantilevers with gold-coated [AU] and amino-modified [NH3] borosilicate glass [GS] particles [PT], 5 µm particle diameter, 0.01 N m^{-1} spring constant, Novascan Technologies, Ames, IA, USA) were used and reacted with SDA and DEX70 according to the steps described for the surface modification. Minor adjustments were made to avoid damaging the sensitive cantilevers or losing the spherical tips. Thus, a special self-built mount for easier handling was used, that allowed up to four cantilevers to be fixed and modified at the same time. Rinsing of the cantilevers was performed by aiming at the cantilever-fixing screws of the holder and never directly at the cantilevers. Before rinsing, the cantilever holder was immersed in ultrapure water twice for 5 min after SDA coupling or 10 min after DEX70 coupling. After rinsing, the residual solvent was removed by patting the holder on a lint-free paper and then placing it under vacuum (10^{-3} mbar) for 1 min (no hot plate!).

Fluorescence Microscopy: All fluorescence images were recorded with the ZEISS Axioskop 2 MOT (Carl Zeiss Microscopy, Oberkochen, Germany) and the associated measurement and evaluation software ZEN (blue edition). The ZEISS objectives Plan-Neofluar 5×/0.15 (item no. 440320-9901-000) and Plan-Neofluar 20×/0.50 Ph 2 (item no. 420351-9910-000) and the ZEISS Filter Set 09 (item no. 488009-9901-000, Excitation BP 450-490, Beamsplitter FT 510, Emission LP 515) were used. The recordings were made without white balance (reset to default), with a gamma value of 1.00, a black reference, and a shading correction. Microscopy had to be done "blind" with the 20x objective because the dots could not be seen through the ocular or in the digital live image. The fluorescence could only be made visible with the correct display parameters set in the intensity histogram in the ZEN software after the image was taken.

XPS: All XPS analyzes were performed in ultrahigh vacuum (multichamber system from PREVAC with a base pressure below 5×10^{-10} mbar) using the hemispherical energy analyzer PHOIBOS 150 (SPECS Surface Nano Analysis GmbH, Berlin, Germany) and a non-monochromatized Mg(Kα) X-Ray source. The XPS spectra were recorded with the associated measurement software SPECS Prodigy. The software CasaXPS (version 2.3.24)[72] was used for the evaluation. The detail spectra were smoothed before determining the bond states. The charge correction was performed analogously to Beamson and Briggs[73] by setting the C–C/C–H bond state of the C 1s signal to 285.0 eV. For the peak fitting, a Shirley background and the Gauss–Lorentz function GL(30) (Gauss–Lorentz product formula with 30% Lorentz portion) with defined peak boundaries and constraints were used. The peaks were assigned using the freely accessible online NIST XPS database,[63] the book by Beamson and Briggs,[73] and selected publications.[64–66,74]

SFM/SFS: All measurements were made with the Molecular Force Probe MFP-3D (Asylum Research Corporation, Oxford Instruments, Santa Barbara, CA, USA) and the associated software AR16 (template from Asylum Research for Igor Pro 6.38B01 from WaveMetrics, Inc., Portland, OR, USA). The cantilevers were calibrated using the Sader method for the resonant frequencies and the thermal tune method for the spring constants. To determine the surface topography parameters, 10×10 µm^2 images were acquired in AC mode with "OMCL-AC160TS" cantilevers (7 nm tip radius, 300 kHz, 26 N m^{-1}, Olympus Corporation, Tokyo, Japan), a resolution of 512 points and lines, a set point of <200 mV, and a scan rate of 0.6–0.8 Hz. To determine layer thicknesses, the scratch method was used (see Section S2, Supporting Information). First, a 1×1 µm^2 image was recorded multiple times in contact mode with the AC mode "All-in-One DLC" cantilever (tip D, 15 nm tip radius, 350 kHz, 40 N m^{-1}, BudgetSensors, Sofia, Bulgaria), a force of 100 nN, a resolution of 256 points and lines, and a scan rate 5.0 Hz until the image no longer changed (usually a maximum of five images). Then, with the same cantilever, a 10×10 µm^2 image was recorded in AC mode with a resolution of 256 points and lines, a set point of 800 mV, and a scan rate of 1.0 Hz (the parameters were not optimized for layer thickness determination). For SFS measurements, the "PT.GS.AU.NH3" cantilevers (see previous section, Tip Modification) were used as received or after modification with DEX70. The measurements were performed on silicon substrates (see previous section, Silicon Surfaces) within the "Closed Fluid Cell Lite" (Asylum Research) in sodium phosphate-buffered saline (pH 7, 4.1 mM NaH_2PO_4, 5.9 mM Na_2HPO_4, 78 mM NaCl, 100 mM ionic strength) with a trigger force of 1 nN and a retraction speed of 2 µm s^{-1}. The image and force-distance curve analysis was made with the software MountainsSPIP Premium v9 (Digital Surf, Besançon, Frankreich). The images were corrected by line-wise leveling (first-order LS polynomial in *x*-direction) and removal of the device-related parabola form (if not already done by the measurement software). The surface topography parameters were output by the software. The layer thicknesses were determined by averaged line profiles laid over the removed areas. For a better representation of the "scratch images," threshold adjustment was used to replace the high signals around the removed areas by non-measured points. All adhesion forces and rupture lengths determined by the force curve analysis were arithmetically averaged (assuming a normal distribution). Pure tip or linker adhesion was excluded for DEX70. The mean adhesion forces F were normalized by dividing them by the tip radius R (2.5 µm) specified by the manufacturer ($F_{norm} = F/R$ with the SI unit N m^{-1}).

Supporting Information

Supporting Information is available from the Wiley Online Library or from the author.

Acknowledgements

The authors gratefully acknowledge the Deutsche Forschungsgemeinschaft (DFG) for the financial support of the projects ZI 487/23-1 and HA 2718/24. The authors also thank Ann-Cathrin Schlapp and Nina Burmeister for their help with preparative work and SFM measurements and Stefan Lach for the acquisition of the XPS spectra.

Open Access funding enabled and organized by Projekt DEAL.

Conflict of Interest

The authors declare no conflict of interest.

Data Availability Statement

The data that support the findings of this study are available from the corresponding author upon reasonable request.

Keywords

dextran, neutral polysaccharides, oral conditioning film, photochemical coupling, scanning force spectroscopy, tip modification

Received: November 29, 2022
Revised: March 2, 2023
Published online: May 23, 2023

[1] R. S. Preethanath, N. W. AlNahas, S. M. Bin Huraib, H. O. Al-Balbeesi, N. K. Almalik, M. H. N. Dalati, D. D. Divakar, *Microb. Pathogen.* **2017** *106*, 20.
[2] N. B. Pitts, D. T. Zero, P. D. Marsh, K. Ekstrand, J. A. Weintraub, F. Ramos-Gomez, J. Tagami, S. Twetman, G. Tsakos, A. Ismail, *Nat. Rev. Disease Primers* **2017**, *3*, 17030.
[3] J. D. B. Featherstone, *Austr. Dent. J.* **2008**, *53*, 286.
[4] C. Hannig, M. Hannig, *Clin. Oral Investig.* **2009** *13*, 123.
[5] K. Kriebel, C. Hieke, B. Müller-Hilke, M. Nakata, B. Kreikemeyer, *Front. Microbiol.* **2018**, *9*, 53.
[6] H. Kanematsu, D. M. Barry, *Biofilm Mater. Sci. 145*, **2015**, 9.
[7] W. Teughels, N. van Assche, I. Sliepen, M. Quirynen, *Clin. Oral Implants Res.* **2006**, *17*, 68.
[8] M. Hannig, C. Hannig, *Oralprophylaxe Kinderzahnheilkunde*. **2007**, *29*, 73.
[9] R. M. Donlan, J. W. Costerton, *Clin. Microbiol. Rev.* **2002**, *15*, 167.
[10] H.-C. Flemming, J. Wingender, *Nat. Rev. Microbiol.* **2010**, *8*, 623.
[11] M. Hannig, A. Joiner, *Monogr. Oral Sci.* **2006**, *19*, 29.
[12] C. Hannig, A. Ruggeri, B. Al-Khayer, P. Schmitz, B. Spitzmüller, D. Deimling, K. Huber, W. Hoth-Hannig, W. H. Bowen, M. Hannig, *Arch. Oral Biol.* **2008**, *53*, 1003.
[13] D. Klemm (ed.), *Polysaccharides II*, Springer-Verlag Berlin Heidelberg, Berlin, Heidelberg **2006**.
[14] M. Rabe, D. Verdes, S. Seeger, *Adv. Colloid Interface Sci.* **2011**, *162*, 87.
[15] W. Norde, *Colloids Surf. B: Biointerfaces* **2008**, *61*, 1.
[16] E. A. Vogler, *Biomaterials* **2012**, *33*, 1201.
[17] P. Somasundaran, S. Krishnakumar, *Colloids Surf. A: Physicochem. Eng. Asp.* **1997**, *123–124*, 491.
[18] H. Stadler, M. Mondon, C. Ziegler, *Analyt. Bioanalyt. Chem.* **2003**, *375*, 53.
[19] C. Müller, J. Wald, W. Hoth-Hannig, N. Umanskaya, D. Scholz, M. Hannig, C. Ziegler, *Analyt. Bioanalyt. Chem.* **2011**, *400*, 679.
[20] F. Bernsmann, N. Lawrence, M. Hannig, C. Ziegler, H. Gnaser, *Analyt. Bioanalyt. Chem.* **2008**, *391*, 545.
[21] M. Wilhelmi, C. Müller, C. Ziegler, M. Kopnarski, *Analyt. Bioanalyt. Chem.* **2011**, *400*, 697.
[22] P. K. Smith, R. I. Krohn, G. T. Hermanson, A. K. Mallia, F. H. Gartner, M. D. Provenzano, E. K. Fujimoto, N. M. Goeke, B. J. Olson, D. C. Klenk, *Analyt. Biochem.* **1985**, *150*, 76.
[23] D. Shugar, *Biochim. Biophys. Acta* **1952**, *8*, 302.
[24] F. Kratz, C. Müller, N. Körber, N. Umanskaya, M. Hannig, C. Ziegler, *Phys. Status Solidi A.* **2013**, *210*, 964.
[25] F. Kratz, S. Trautmann, N. Umanskaya, C. Müller-Renno, M. Hannig, C. Ziegler, *Phys. Status Solidi A* **2016**, *213*, 1486.
[26] C. Rösch, F. Kratz, T. Hering, S. Trautmann, N. Umanskaya, N. Tippkötter, C. Müller-Renno, R. Ulber, M. Hannig, C. Ziegler, *Colloids Surf. B: Biointerfaces* **2017**, *149*, 115.
[27] C. Müller, A. Lüders, W. Hoth-Hannig, M. Hannig, C. Ziegler, *Langmuir* **2010**, *26*, 4136.
[28] N. Schwender, K. Huber, F. A. Marrawi, M. Hannig, C. Ziegler, *Appl. Surf. Sci.* **2005**, *252*, 117.
[29] C. Rösch, C. Huber, C. Müller, N. Umanskaya, M. Hannig, C. Ziegler, *Phys. Status Solidi A* **2013**, *210*, 945.
[30] M. DuBois, K. Gilles, J. K. Hamilton, P. A. Rebers, F. Smith, *Nature* **1951**, *168*, 167.
[31] M. DuBois, K. A. Gilles, J. K. Hamilton, P. A. Rebers, F. Smith, *Anal. Chem.* **1956**, *28*, 350.
[32] P. Arenja, C. Rösch, K. Huttenlochner, C. Müller-Renno, M. Hannig, C. Ziegler, *Phys. Status Solidi A* **2018**, *215*, 1700845.
[33] S. Ehnert, J. Seehase, C. Müller-Renno, M. Hannig, C. Ziegler, *Analyt. Chim. Acta* **2021**, *1174*, 338712.
[34] M. Frasconi, F. Mazzei, T. Ferri, *Analyt. Bioanalyt. Chem.* **2010**, *398*, 1545.
[35] S. K. Vashist, E. Lam, S. Hrapovic, K. B. Male, J. H. T. Luong, *Chem. Rev.* **2014** *114*, 11083, .
[36] R. Barattin, N. Voyer, *Chem. Commun.* **2008**, 1513.
[37] B. J. Jones, A. Mahajan, A. Aksan, *PloS One* **2019**, *14*, 0222006.
[38] A. S. Volokhova, K. J. Edgar, J. B. Matson, *Mater. Chem. Front.* **2020** *4*, 99.
[39] O. Rief, G. Heymann, *Science* **1997**, *275*, 1295.
[40] P. E. Marszalek, H. Li, A. F. Oberhauser, J. M. Fernandez, *Proc. Natl. Acad. Sci. USA* **2002**, *99*, 4278.
[41] K. A. Walther, J. Brujić, H. Li, J. M. Fernández, *Biophys. J.* **2006**, *90*, 3806.
[42] A. Fellah, N. Belmiloud, R. G. Haverkamp, Y. Hemar, D. Otter, M. A. K. Williams, *Carbohydr. Polym.* **2012**, *87*, 806.
[43] G. Elender, M. Kühner, E. Sackmann, *Biosens. Bioelectron.* **1996**, *11*, 565.
[44] L. Ding, W. Cheng, X. Wang, S. Ding, H. Ju, *J. Am. Chem. Soc.* **2008**, *130*, 7224.
[45] N. Laurent, J. Voglmeir, S. L. Flitsch, *Chem. Commun.* **2008**, 4400.
[46] S. Park, J. C. Gildersleeve, O. Blixt, I. Shin, *Chem. Soc. Rev.* **2013**, *42*, 4310.
[47] Q. Liu, Y. Zhang, J. S. Laskowski, *Int. J. Miner. Process.* **2000**, *60*, 229.
[48] J. S. Laskowski, Q. Liu, C. T. O'Connor, *Int. J. Miner. Process.* **2007**, *84*, 59.
[49] J. L. Wood, *Biochem. J.* **1974**, *143*, 775.
[50] K. Gruber, T. Horlacher, R. Castelli, A. Mader, P. H. Seeberger, B. A. Hermann, *ACS Nano* **2011**, *5*, 3670.
[51] S. F. Musolino, Z. Pei, L. Bi, G. A. DiLabio, J. E. Wulff, *Chem. Sci.* **2021**, *12*, 12138.
[52] A. L. Mackinnon, J. Taunton, *Curr. Protocols Chem. Biol.* **2009**, *1*, 55.
[53] A. F. Gomes, F. C. Gozzo, *J. Mass Spectrom.* **2010**, *45*, 892.
[54] S. A. Weissman, D. Zewge, *Tetrahedron* **2005**, *61*, 7833.

[55] B. C. Ranu, S. Bhar, *Org. Prep. Procedur. Int.* **1996** *28*, 371.
[56] R. M. Smith, D. E. Hansen, *J. Am. Chem. Soc.* **1998** *120*, 8910.
[57] A. R. Yadav, R. Sriram, J. A. Carter, B. L. Miller, *Mater. Sci. Eng. C, Mater. Biol. Appl.* **2014**, *35*, 283.
[58] X. Yuan, N. Wolf, D. Mayer, A. O. Usser, R. W. Rdenweber, *Langmuir* **2019**, *35*, 8183.
[59] W.-M. Munief, F. Heib, F. Hempel, X. Lu, M. Schwartz, V. Pachauri, R. Hempelmann, M. Schmitt, S. Ingebrandt, *Langmuir* **2018**, *34*, 10217.
[60] M. Zhu, M. Z. Lerum, W. Chen, *Langmuir* **2012**, *28*, 416.
[61] J. K. Armstrong, R. B. Wenby, H. J. Meiselman, T. C. Fisher, *Biophys. J.* **2004**, *87*, 4259.
[62] T. L. Barr, S. Seal, *J. Vac. Sci. Technol. A: Vac. Surf. Films* **1995**, *13*, 1239.
[63] C. Powell, X-Ray Photoelectron Spectroscopy Database XPS,Version 4.1, NIST Standard Reference Database 20, National Institute of Standards and Technology **1989**.
[64] D. V. Okhrimenko, A. Budi, M. Ceccato, M. Cárdenas, D. B. Johansson, D. Lybye, K. Bechgaard, M. P. Andersson, S. L. S. Stipp, *ACS Appl. Mater. Interfaces* **2017**, *9*, 8344.
[65] K. M. Kallury, R. F. Debono, U. J. Krull, M. Thompson, *J. Adhes. Sci. Technol.* **1991**, *5*, 801.
[66] B. Luo, J. E. Rossini, W. L. Gladfelter, *Langmuir* **2009**, *25*, 13133.
[67] W. Sung, Z. Avazbaeva, D. Kim, *J. Phys. Chem. Lett.* **2017** *8*, 3601.
[68] M. Appell, G. Strati, J. L. Willett, F. A. Momany, *Carbohydr. Res.* **2004**, *339*, 537.
[69] I. M. Neelov, D. B. Adolf, T. C. B. McLeish, E. Paci, *Biophys. J.* **2006**, *91*, 3579.
[70] D. Alsteens, A. Beaussart, S. El-Kirat-Chatel, R. M. A. Sullan, Y. F. Dufrêne, *PLoS Pathogens* **2013** *9*, 1003516.
[71] J. Zlatanova, *Progr. Biophys. Mol. Biol.* **2000**, *74*, 37.
[72] N. Fairley, V. Fernandez, M. Richard-Plouet, C. Guillot-Deudon, J. Walton, E. Smith, D. Flahaut, M. Greiner, M. Biesinger, S. Tougaard, D. Morgan, J. Baltrusaitis, *Appl. Surf. Sci. Adv.* **2021**, *5*, 100112.
[73] G. Beamson, D. Briggs, in *High Resolution XPS Of Organic Polymers*, Wiley, Chichester **1992**.
[74] P. Post, L. Wurlitzer, W. Maus-Friedrichs, A. P. Weber, *Nanomaterials* **2018**, *8*, 530.
[75] Avogadro Chemistry, Powered by Jekyll & Minimal Mistakes, Avogadro: An Open-Source Molecular Builder and Visualization Tool.
[76] M. D. Hanwell, D. E. Curtis, D. C. Lonie, T. Vandermeersch, E. Zurek, G. R. Hutchison, *J. Cheminform.* **2012**, *4*, 17.